Nonlocal phase modulation of multimode, continuous-variable twin beams

Zhifan Zhou,[1] Luís E. E. de Araujo,[1,2] Matt DiMario,[1] B. E. Anderson,[3] Jie Zhao,[1] Kevin M. Jones,[4] and Paul D. Lett[1,5,*]

[1] *Joint Quantum Institute, National Institute of Standards and Technology and the University of Maryland, College Park, Maryland 20742, USA*
[2] *Institute of Physics Gleb Wataghin, University of Campinas (UNICAMP), 13083-859 Campinas, São Paulo, Brazil*
[3] *Department of Physics, American University, Washington DC 20016, USA*
[4] *Department of Physics, Williams College, Williamstown, Massachusetts 01267, USA*
[5] *Quantum Measurement Division, National Institute of Standards and Technology, Gaithersburg, Maryland 20899, USA*

(Dated: January 9, 2023)

Multimode entanglement is a key resource in quantum information processing and quantum metrology, such as high dimensional cluster-state generation and distributed quantum sensing. At the same time, quantum nonlocality is a remarkable feature of quantum theory and has applications in quantum teleportation and Bell inequality tests. Exploring the intersection of these two aspects of quantum theory, we here investigate experimentally the nonlocal phase modulation of multimode, continuous-variable entangled twin beams. We modulate the phase of the entangled probe and conjugate beams of light, produced in a four-wave mixing interaction in hot Rb vapor, with a pair of electro-optical phase modulators. While a single-phase modulator in either one of the twin beams reduces the entanglement (squeezing) signal, we find that the pair of modulators interfere nonlocally to modify the beam correlations. The nonlocal modulation of the beams creates quantum correlations among frequency modes of the multimode fields.

In recent years, multimode entanglement has attracted great interest in quantum computing [1–3], quantum metrology [4–6], and quantum information processing in general [7]. Examples include Gaussian-Bose sampling [8–10] and distributed quantum sensing [4–6], which rely on linear mixing and splitting of squeezed light sources. The technical challenge in these applications increases as the number of modes increases. Multimode entanglement in the frequency domain, such as in quantum optical frequency combs [11–14], provides scalable and compact sources for those applications.

A remarkable feature of quantum theory is the concept of nonlocality, whereby entangled particles interact even when separated by large distances. For a pair of entangled photons, the nonlocal character of quantum theory can manifest itself through Bell inequality tests [15–17], as well other effects such as nonlocal dispersion cancellation [18, 19], nonlocal quantum erasing [20], nonlocal aberration cancelation [21], and nonlocal phase modulation [22, 23].

Twin beams play an important role in continuous-variable (CV) quantum information processing [24] by enabling deterministic generation, manipulation, and detection of entangled light. The generation and control of CV entangled states of light find many applications in quantum erasing [25, 26], quantum steering [27], quantum imaging [28], quantum key distribution protocols [29], and cluster-state based quantum computing [30], among others. The electro-optical phase modulator (EOM) is a key element in many of these schemes. At the classical level, the ideal EOM simply provides a temporal phase modulation of the complex envelope of the incident light field, resulting in the generation of spectral sidebands if the modulation is periodic. Recent works employ an EOM for generating high-dimensional quantum states [30].

In this Letter, we experimentally investigate the effect of nonlocal phase modulation of multifrequency modes entangled CV beams. In nonlocal phase modulation, two distant EOMs, each operating on one of a pair of entangled fields, act cumulatively to determine the apparent modulation depth. Nonlocal modulation in the discrete-variable (DV) regime is observed in the intensity correlations between spatially-separated entangled twin photons [23]. In the CV framework explored here, we are concerned with amplitude correlations and phase correlations between quadrature amplitudes of the twin fields. We describe our investigation into how an EOM affects the squeezing signal between twin beams and how the relative phase between a pair of EOMs, each acting on one of the twin beams, changes the correlations between neighboring frequency modes of the conjugate joint field quadratures.

We consider two-mode squeezed states produced in the double-lambda, four-wave-mixing (4WM) scheme illustrated in Fig. 1. For input fields $\hat{a}_p$ (probe) and $\hat{a}_c$ (conjugate) entering the 4WM medium, the output fields are:

$$\hat{A}_p = G\hat{a}_p + g\hat{a}_c^\dagger \tag{1}$$

$$\hat{A}_c = G\hat{a}_c + g\hat{a}_p^\dagger, \tag{2}$$

where G is the amplitude gain, and $g^2 = G^2 - 1$. To express the fields after they go through the EOMs, we consider a simple classical model for the phase modulators [31]. We assume both phase modulators are ideal and are periodically modulated at the same modulation frequency Ω. In the time domain, the EOM's

transfer functions are $h_i(t) = \exp[i\pi m_i\, g_i(t)]$, where $i = p, c$ (p or c for probe or conjugate, respectively); m_i is the modulation depth; and $g_i(t) = \sin(\Omega t + \phi_i)$, with ϕ_i being a driving phase. The exit fields are then: $\hat{A}'_p = \exp[i\pi m_p g_p(t)]\hat{A}_p$ and $\hat{A}'_c = \exp[i\pi m_c g_c(t)]\hat{A}_c$. We can then define the joint quadrature operators: $\hat{X}_\pm = (\hat{X}_p \pm \hat{X}_c)/\sqrt{2}$ and $\hat{P}_\pm = (\hat{P}_p \pm \hat{P}_c)/\sqrt{2}$, where $\hat{X}_{p,c} = (\hat{A}'_{p,c} + \hat{A}'^{\dagger}_{p,c})/\sqrt{2}$ and $\hat{P}_{p,c} = -i(\hat{A}'_{p,c} - \hat{A}'^{\dagger}_{p,c})/\sqrt{2}$ are the usual amplitude and phase quadratures, respectively, of the fields. The noise of the joint quadratures can be calculated and is found to be

$$\langle X_-^2\rangle = \frac{1}{2}\{G^2 + g^2 - 2gG \times \cos[\pi(m_p \sin\varphi + m_c \sin(\varphi+\phi))]\}, \tag{3}$$

where $\varphi = \varphi(t) = \Omega t + \phi_p$, and $\phi = \phi_c - \phi_p$ is the phase difference between the two EOMs. Averaging over one modulation period gives

$$\langle \overline{X_-^2}\rangle = \frac{1}{2}\Big\{G^2 + g^2 - 2gG \times J_0\left(\pi\sqrt{m_p^2 + m_c^2 + 2m_p m_c\cos\phi}\right)\Big\}, \tag{4}$$

where J_0 is a zeroth order Bessel function, and the overbar represents a time average. It is straightforward to show that $\langle \overline{P_+^2}\rangle = \langle \overline{X_-^2}\rangle$. If the modulation depth of the EOMs is equal ($m_p = m_c = m$), then

$$\langle \overline{X_-^2}\rangle = \frac{1}{2}\left\{G^2 + g^2 - 2gGJ_0\left(\pi m\sqrt{2+2\cos\phi}\right)\right\}. \tag{5}$$

If both EOMs are turned off ($m = 0$), then $\langle \overline{X_-^2}\rangle = (G-g)^2/2$. For any $G^2 > 1$, two-mode squeezing is observed since this implies $\langle \overline{X_-^2}\rangle < 1/2$, which is the shot-noise level (SNL). In deriving Eq. (5), we made no assumptions regarding the spatial separation of modes $\hat{a}_p$ and $\hat{a}_c$. Equation (5) implies that maximum squeezing between the two fields is obtained when the two phase modulators are off. Turning the modulators on will, in general, reduce the degree of squeezing. For a high enough modulation depth, squeezing may be eliminated as the quadrature noise will exceed the SNL.

Three cases are particularly of interest: the EOMs drove in ($\phi = 0°$) and out ($\phi = 180°$ and $\phi = 120°$) of phase with each other. When $\phi = 180°$, Eq. (5) clearly shows that the modulation imparted to one of the twin beams cancels the modulation experienced by the other twin beam; and two-mode squeezing, at the same level as obtained with the EOMs off, is recovered. Comparing Eqs. (4) and (5), we see that, when the two EOMs are in phase, they produce the same amount of squeezing as only one modulator operating at twice the modulation depth ($m_p = 0$ and $m_c = 2m$, or vice-versa). And for $\phi = 120°$, Eq. (5) predicts that the two EOMs should behave as a single modulator driven at a modulation depth of m. More generally, the effect of two-phase modulators on the joint quadrature noise is similar to that of a single modulator operating at an effective modulation depth of $\sqrt{m_p^2 + m_c^2 + 2m_p m_c\cos\phi}$. In other words, the modulators act cumulatively to determine the effective modulation depth, analogously to the DV case [22, 23]. The cumulative effect is nonlocal. That is, it is independent of the distance between the EOMs.

Figure 1 shows the experimental setup and a level diagram of the double-lambda 4WM scheme. The setup is similar to the one described in [28]. A 12 mm-long Rb vapor cell is heated to 123°C. A single pump beam, tuned to the ^{85}Rb D_1 line, is split into two beams: one is sent through the vapor cell along with a probe seed beam to generate the local oscillator (LO) beams, and the other generates the two-mode squeezed vacuum states. The probe seed is derived from the pump beam by double passing a small portion of the pump through a 1.5 GHz acoustic-optic modulator. The pump and probe intersect inside the cell at an angle of 7 mrad. A double-lambda 4WM process uses the $\chi^{(3)}$ nonlinearity of the Rb vapor to convert two pump photons into one probe photon and one conjugate photon. (The squeezed beams are vacuum seeded.). The probe beam experiences a typical gain of 3. The non-degenerate probe and conjugate beams are on opposite sides of the pump and in a two-mode squeezed state. Probe and conjugate beams pass through identical EOMs driven with a 200 kHz sine wave. The EOMs are driven synchronously by separate outputs of the same function generator, and their relative phase can be adjusted by the function generator. To provide access to measurements of the phase quadrature, the modulated probe and conjugate beams are sent separately to two balanced homodyne detectors, one for the probe and another for the conjugate.

In the homodyne detectors, the probe and conjugate beams are mixed with a LO beam on a 50/50 beamsplitter with fringe visibilities > 97%. The relative phases $\theta_{p,c}$ between the LOs and the probe/conjugate fields are adjusted by mirrors mounted on piezoelectric transducers (PZT) in order to select the quadrature to be detected in each beam. The outputs of the homodyne detectors are directly measured with matched photodiodes with quantum efficiencies of 95%. The path length from the vapor cell to the optical detectors for probe and conjugate beams are approximately matched. However, due to the different group velocities of the probe and conjugate beams in the atomic vapor [32], the two fields are optically delayed by approximately 10 ns. To compensate for this delay, we add an electronic delay line after detection by adjusting the relative BNC cable lengths. The photocurrents are amplified and then measured with a 1 GHz digital sampling oscilloscope. The measured time traces are digitally post-processed in order to determine the power spectrum and joint quadratures of the twin

beams.

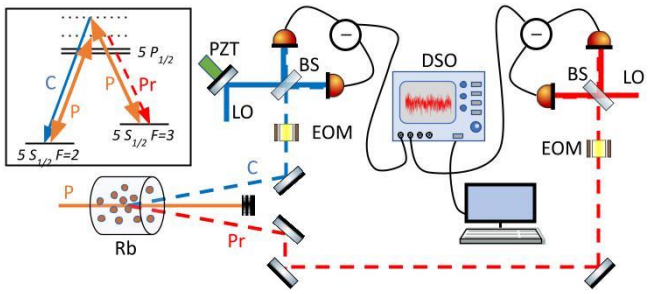

FIG. 1. Experimental setup and energy level diagram (inset) of the 4WM process in ^{85}Rb. The pump beam (P) generates twin probe (Pr) and conjugate beams (C) in a two-mode squeezed state. BS are 50/50 nonpolarizing beamsplitters; EOMs are electro-optical phase modulators; PZT is a piezoelectric transducer; DSO is a 1 GHz digital sampling oscilloscope; and LO are local oscillator fields for the homodyne detection schemes.

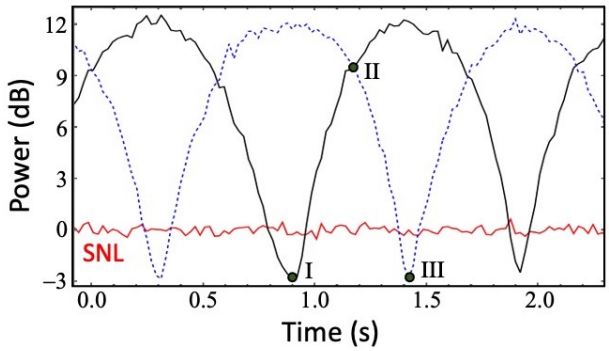

FIG. 2. Noise power of the sum (dashed blue) and difference (solid black) of the quadratures measured by the homodyne detectors as the phase θ is varied. In both cases, the noise is analysed at a frequency of 1 MHz. By locking the phase to points I ($\theta = 0$), II ($\theta = \pi/4$) or III ($\theta = \pi/2$), we can measure the joint quadratures XX, XP or PP, respectively, of the twin beams.

The homodyne signal as a function of local oscillator phase gives a generalized quadrature: $\hat{X}_i \cos\theta_i + \hat{P}_i \sin\theta_i$. If we subtract the homodyne signals, we measure the noise power of the joint quadrature $\hat{X}_\theta = \hat{X}_{\theta_p} - \hat{X}_{\theta_c}$, where $\theta = \theta_p + \theta_c$. A typical noise spectrum as a function of the phase θ is shown in Fig. 2. Squeezing is observed when $\theta = 0$ (point I in the figure). A frequency-dependent squeezing spectrum is observed by locking the LO phase θ to point I by a noise locking technique [33]. (Locking the phase to point III, would give us the quadrature $\hat{P}_\theta = \hat{P}_{\theta_p} - \hat{P}_{\theta_c}$.) Because the temporal modulation imparted by the EOMs to the beams may disturb the locking signal, we pulse the driving signal from the function generator to the EOMs at 40 Hz. The driving pulses are square pulses with a width of 12.5 ms. The noise of the subtracted photocurrents therefore alternates between the squeezing signal observed with the EOMs on and with the EOMs off. The signals from the probe and conjugate homodyne detectors consisted of 10^6 values sampled over 10 ms captured during the time the EOMs were on. The measurement window of 10 ms is purposely smaller than the pulse width in order to avoid transient edge effects in the data. We then used Welch's method [34] to obtain the final power spectrum of the measured noise.

Typical squeezing spectra are shown in Fig. 3. When the EOMs are off (Fig. 3a), the squeezing spectrum extends over a bandwidth of approximately 15 MHz. Turning one EOM on (on either the probe or conjugate beam) reduces squeezing at all frequencies. At twice the modulation depth, squeezing is eliminated, with the noise well above SNL. When both EOMs are on, the effect of the EOMs on the nonlocal entangled signal depends on their relative phase (Fig. 3b). When the EOMs are in phase, they act together to reduce the squeezing signal, producing a spectrum similar to that of a single EOM with twice the modulation depth acting on only one of the beams (shown in Fig. 3a). When the EOMs are 180° out of phase, they cancel each other, giving a squeezing signal similar to that observed when the EOMs are turned off. And when the EOMs are dephased by 120°, the squeezing spectrum is similar to the spectrum seen with only one EOM on. These results are in complete agreement with the predictions of our model. They are the CV analog of the nonlocal modulation effect reported in Ref. [23] in the DV regime.

We next studied the dependence of the squeezing signal (variance of $\hat{X}_-$) on the relative phase difference ϕ of the EOMs. To calculate $\langle\overline{\hat{X}_-^2}\rangle$, we first broke the measured time traces into 2000 equal-size, nonoverlapping segments of 5 μs, then applied a strategy similar to the one described in Ref. [35] to each segment. We spectrally filtered $\hat{X}_-$ by multiplying the time segments by the window function: $W(t) = (1/\sigma\sqrt{2\pi})\cos[\omega_0(t-t_0)]\exp[-(t-t_0)^2/2\sigma^2]$, where t_0 is the midpoint of the temporal segment, σ is the window width, and ω_0 is the center frequency of the limited bandwidth where the squeezing is maximized. We integrated each filtered segment to obtain 2000 values of $\hat{X}_-$. We then calculated the variance of these values to obtain $\langle\overline{X_-^2}\rangle$. Figure 4 shows the normalized noise variance of X_- (relative to shot noise) as a function of ϕ. We see that the noise variance, initially above SNL for $\phi = 0°$, decreases with increasing phase, dropping below SNL for $\phi \gtrsim 120°$. The noise variance is smallest at 180° phase difference, where it coincides with the variance measured when the EOMs are off, within experimental uncertainty. Equation (5) describes well the experimental data. A fit of Eq. (5) to the data gives $m = 0.18$ and $G^2 \approx 3.2$; these values are in close agreement with the applied modulation depth ($m = 0.12$) and estimates of the probe gain. The small disagreement between the fitted curve and experimental data are likely

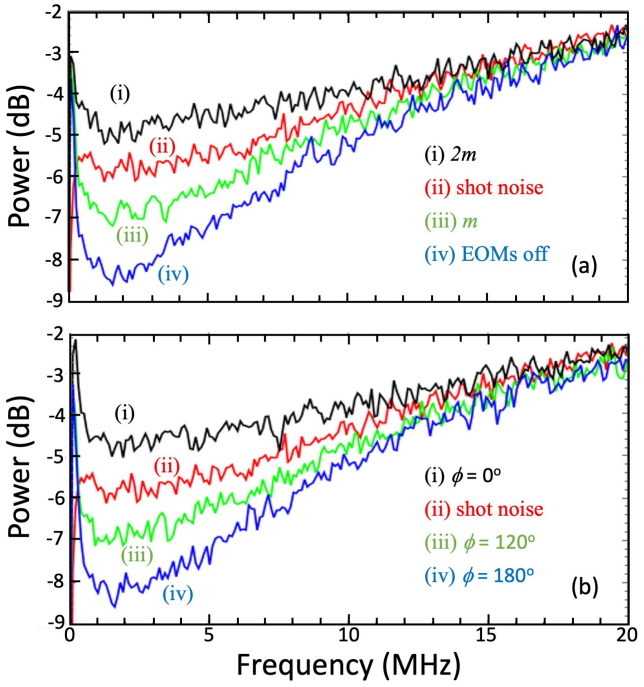

FIG. 3. (a) Squeezing spectra obtained with both EOMs turned off (blue line) and with one EOM on, but at different modulation depths: m (green line) and $2m$ (black line); (b) Squeezing spectra for both EOMs running, at a modulation depth m, in phase ($\phi = 0°$) and out of phase ($\phi = 180°$ and $\phi = 120°$). In all cases, $m = 0.096$ and the red line indicates the shot noise. A plot of typical squeezing and shot noise spectra along with the electronic noise can be found in the Supplemental Material.

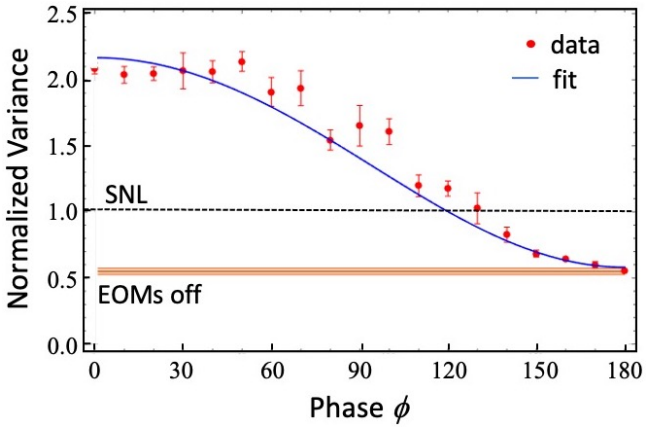

FIG. 4. Joint quadrature variance $\langle \overline{X_-^2} \rangle$ normalized by the shot noise variance as a function of the phase difference ϕ between the EOMs. The solid blue line is a fit of Eq. (5) to the experimental data (red full circles): $f(t) = 2a - 1 - 2\sqrt{a-1} * \sqrt{a} J_0(\pi b \sqrt{2+2\cos\phi}) + c$, with fit parameters $a = 3.2$, $b = 0.18$ and $c = 0.49$; c is an offset added to partially account for losses in the system. The dotted black line is the shot noise level (SNL). For the window function used to filter the temporal data, we used: $W(t) = (1/\sigma\sqrt{2\pi})\cos[\omega_0(t - t_0)]\exp[-(t-t_0)^2/2\sigma^2]$, with $\sigma = 10\,\mu$s and $\omega_0 = 2\pi \times 1$ MHz. Also shown is the measured variance when the EOMs are off; the width of the colored band corresponds to the measurement uncertainty. Uncertainty bars are one standard deviation.

due to the simplicity of the model that, for example, does not include the unavoidable losses in the experiment [36]. Another important source of disagreement is related to mechanical drifts of the homodyne optical setups during data acquisition, which reduce the fringe visibilities and increase the noise variances.

Full characterization of the two-mode squeezed states requires determining the covariance matrix C of the fields. In the ordered basis $(\hat{X}_p, \hat{X}_c, \hat{P}_p, \hat{P}_c)$:

$$C = \begin{bmatrix} C_{XX} & C_{XP} \\ (C_{XP})^T & C_{PP} \end{bmatrix}, \tag{6}$$

where C_{XX}, C_{XP}, and C_{PP} are 2×2 matrices. The covariance matrix of the two-mode squeezed state is symmetric. C_{XX} and C_{PP} are associated with the amplitude XX and phase PP joint quadratures of the twin beams, respectively, while C_{XP} is the mutual correlation matrix between their X and P quadratures. When the EOMs are off, $C_{XP} = 0$, so the covariance matrix is block diagonal. Turning on the phase modulators couples the X and P quadratures of the fields, and $C_{XP} \neq 0$.

We can gain further insight into the characteristics of the nonlocal modulation of the EOMs by measuring the XP quadrature of the covariance matrix for the twin beams. In order to do that, we lock the joint quadrature phase to $\theta = \pi/4$ (point II in Fig.2). The locking scheme is detailed in the Supplemental Material. We detected the noise signal of the probe and conjugate beams with the same homodyne detection technique previously described. To recover the XP covariance matrix from the acquired time traces at different frequency modes, we need to filter frequency bins for analysis. That is, all the noise whose frequencies are contained in an interval $[\omega - \Delta\omega/2, \omega + \Delta\omega/2]$ is grouped into a single frequency bin of width $\Delta\omega$ and centered on frequency ω. The temporal data is Fourier transformed to the frequency domain, a 180 kHz rectangular filter is applied to each frequency mode at a time, and then the inverse Fourier is transformed back to the time domain. We thus derived 49 nonoverlapping frequency modes distributed over a bandwidth of 10 MHz at steps of 200 kHz. The filtered probe and conjugate data are joined into one matrix where each column represents the time domain data of a single frequency mode. Calculating the covariance between the 98 columns of that matrix gives a 98x98 covariance matrix quadrant for the XP quadrature of the twin beams.

Figure 5a shows the measured XP covariance matrices. When the beams are not modulated, their X and P quadratures are not coupled. We also do not observe any correlations when the EOMs are operated at 180° phase

difference. However, at 0° phase difference, the X and P quadratures of the probe and conjugate beams are coupled, and positive correlations can be seen. The double diagonal structure in the covariance matrix corresponds to the frequency sidebands introduced by the EOMs and demonstrates the multimode nonclassical nature of the phase-modulated joint field quadratures. A single EOM, at twice the modulation depth, produces similar correlations to those produced by the two in-phase EOMs.

In all results presented so far, both EOMs were placed in the path of the twin beams. This configuration is of interest for quantum information processing applications, such as the production of cluster states or quantum key distribution. However, other applications, such as quantum erasing and distributed quantum sensing, might require the EOMs placed in the LO beams instead, or in a combination of one EOM in a LO beam and the other in one of the twin beams [25, 26]. In Fig. 5(b), we show the results obtained when both EOMs are placed in the LO oscillators' paths. It is clear that the effect of the EOMs on the measured beam correlations is the same as the one observed with the EOMs placed in the beams, except for a change of sign in the correlations. However, placing one EOM on the probe beam and the other EOM on the LO of the conjugate beam causes a different effect on the measured correlations, as shown in Fig. 5(c). In this case, the EOMs cancel each other when they are in phase and couple the X and P quadratures when they are out of phase. These results can be understood by making use of an analogy to an SU(1,1) interferometer. What is generally referred to as an SU(1,1) interferometer [37] would entail twin quantum-correlated beams generated by a nonlinear interaction (such as 4WM), some phase shift on one or both of the twin beams, followed by recombining these beams in a second nonlinear interaction. The phase shift that is read out in such an interferometer is converted to an intensity signal in the second nonlinear interaction region. If the phase at the second interaction $[2\theta_{pump}-(\theta_{probe}+\theta_{conjugate})=\pi]$ is undisturbed, then the probe and conjugate beams are re-converted into pump photons, and no light appears in the probe and conjugate outputs. An additional phase shift appears as a non-zero output intensity in the twin beams. If one views the arrangement in Fig. 1 as a "truncated" version of the SU(1,1) interferometer [38], it can be seen to be a pair of interferometers, both comprised of a (very noisy) signal beam, plus a LO beam. These interferometers will, however, have quantum-correlated signals, and any phase shift written onto one of the beams can be detected at a sub-shot-noise level in the difference. When one views the interferometers in this scheme independently, it is clear that it does not matter if the phase shift is written onto the "signal" beam, or onto the LO beam – either way, the homodyne output contains the signal. Because of the geometry, however, a similar phase shift written on the LO will appear as a phase shift of the opposite sign to one written onto the signal beam. (If the signal and the local oscillator have the same phase shift, the detector will not see it.)

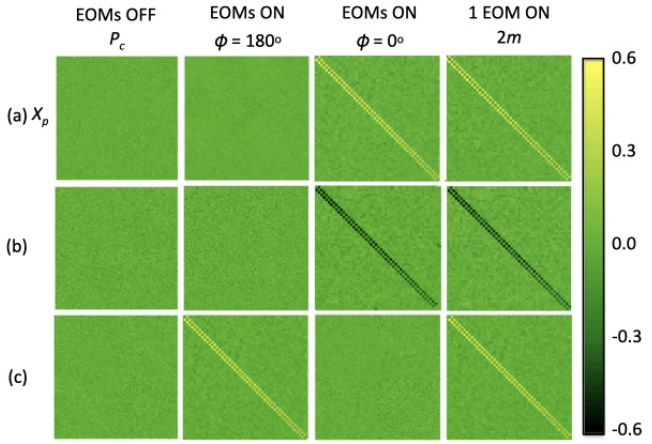

FIG. 5. Measured XP covariance matrices for (a) both EOMs on the twin beams, (b) both EOMs on local oscillator beams and (c) one EOM on the probe beam and the other EOM on conjugate local oscillator. All panels show the $X_p - P_c$ sub-subquadrant of their respective XP covariance matrix. In the two cases where both EOMs are on, their modulation depth is $m = 0.1$. The double diagonal structure of the correlations corresponds to the first-order frequency sidebands due to the periodic modulation of the beams by the EOMs.

In conclusion, we studied the effects of electro-optical phase modulation on two-mode squeezing of multi-mode, continuous variable twin beams. The electro-optical modulators interfered nonlocally to modify the beam correlations, which were controlled by adjusting the relative driving phase of the modulators. We found that the modulators acted cumulatively to determine the effective modulation depth. We believe that our setup is a potential platform for further experimental studies on cluster state generation, quantum erasing, and quantum compressed sensing. As shown here, the ability to manipulate twin beam correlations via nonlocal phase modulation has important implications for those fields. For example, positioning the EOM in the local oscillator should allow the implementation of compressed sensing for quantum system characterization. Positioning the EOMs in the local oscillators also brings an experimental advantage, since it avoids the introduction of additional losses in the signal beams, allowing for larger squeezing signals. A recent proposal for generating hypercubic cluster states suggests using an EOM to couple different frequency qumodes of two-mode entangled beams [30]. Our results make it clear that applying twice the modulation on one EOM is equivalent to an EOM in each entangled beam, at least when it comes to the structure of a cluster state.

This work was supported by the Air Force Office of Scientific Research (FA9550- 16-1-0423).

L. E. E. de Araujo acknowledges the financial support of grant #2019/24743-9, São Paulo Research Foundation (FAPESP). We acknowledge Alessandro Restelli for the help with the lock circuits. This research was performed while Matthew DiMario held a National Research Council Research Associateship Award at NIST.

* Email: lett@umd.edu

[1] S. Yokoyama, R. Ukai, S. C. Armstrong, C. Sornphiphatphong, T. Kaji, S. Suzuki, J. Yoshikawa, H. Yonezawa, N. C. Menicucci, and A. Furusawa, Ultra-large-scale continuous-variable cluster states multiplexed in the time domain, Nature Photonics **7**, 982 (2013).

[2] M. V. Larsen, X. Guo, C. R. Breum, J. S. Neergaard-Nielsen, and U. L. Andersen, Deterministic generation of a two-dimensional cluster state, Science **366**, 369 (2019).

[3] W. Asavanant, Y. Shiozawa, S. Yokoyama, B. Charoensombutamon, H. Emura, R. N. Alexander, S. Takeda, J. Yoshikawa, N. C. Menicucci, H. Yonezawa, and A. Furusawa, Generation of time-domain-multiplexed two-dimensional cluster state, Science **366**, 373 (2019).

[4] X. Guo, C. R. Breum, J. Borregaard, S. Izumi, M. V. Larsen, T. Gehring, M. Christandl, J. S. Neergaard-Nielsen, and U. L. Andersen, Distributed quantum sensing in a continuous-variable entangled network, Nature Physics **16**, 281 (2020).

[5] B. K. Malia, Y. Wu, and M. A. Martínez-Rincón, J.and Kasevich, Distributed quantum sensing with mode-entangled spin-squeezed atomic states, Nature **612**, 661 (2022).

[6] B. C. Nichol, R. Srinivas, D. P. Nadlinger, P. Drmota, D. Main, G. Araneda, C. J. Ballance, and D. M. Lucas, An elementary quantum network of entangled optical atomic clocks, Nature , 689 (2022).

[7] M. Erhard, M. Krenn, and A. Zeilinger, Advances in high-dimensional quantum entanglement, Nature Reviews Physics **2**, 365–381 (2020).

[8] C. S. Hamilton, R. Kruse, L. Sansoni, S. Barkhofen, C. Silberhorn, and I. Jex, Gaussian boson sampling, Phys. Rev. Lett. **119**, 170501 (2017).

[9] F. Arute, K. Arya, R. Babbush, D. Bacon, J. C. Bardin, R. Barends, R. Biswas, S. Boixo, F. G. Brandao, D. A. Buell, *et al.*, Quantum supremacy using a programmable superconducting processor, Nature **574**, 505 (2019).

[10] H.-S. Zhong, H. Wang, Y.-H. Deng, M.-C. Chen, L.-C. Peng, Y.-H. Luo, J. Qin, D. Wu, X. Ding, Y. Hu, *et al.*, Quantum computational advantage using photons, Science **370**, 1460 (2020).

[11] O. Pinel, P. Jian, R. M. de Araújo, J. Feng, B. Chalopin, C. Fabre, and N. Treps, Generation and characterization of multimode quantum frequency combs, Phys. Rev. Lett. **108**, 083601 (2012).

[12] J. Roslund, R. M. De Araujo, S. Jiang, C. Fabre, and N. Treps, Wavelength-multiplexed quantum networks with ultrafast frequency combs, Nature Photonics **8**, 109 (2014).

[13] Y. Cai, J. Roslund, G. Ferrini, F. Arzani, X. Xu, C. Fabre, and N. Treps, Multimode entanglement in reconfigurable graph states using optical frequency combs, Nature communications **8**, 1 (2017).

[14] Y.-S. Ra, A. Dufour, M. Walschaers, C. Jacquard, T. Michel, C. Fabre, and N. Treps, Non-gaussian quantum states of a multimode light field, Nature Physics **16**, 144 (2020).

[15] J. S. Bell, Con the einstein podolsky rosen paradox, Physics Physique Fizika **1**, 195 (1964).

[16] A. Aspect, J. Dalibard, and G. Roger, Experimental test of bell's inequalities using time-varying analyzers, Phys. Rev. Lett. **49**, 1804 (1982).

[17] B. Hensen, H. Bernien, A. E. Dréau, A. Reiserer, N. Kalb, M. S. Blok, J. Ruitenberg, R. F. L. Vermeulen, R. N. Schouten, C. Abellán, W. Amaya, V. Pruneri, M. W. Mitchell, M. Markham, D. J. Twitchen, D. Elkouss, S. Wehner, T. H. Taminiau, and R. Hanson, Loophole-free bell inequality violation using electron spins separated by 1.3 kilometres, Nature **526**, 682 (2015).

[18] J. D. Franson, Nonlocal cancellation of dispersion, Phys. Rev. A **45**, 3126 (1992).

[19] S.-Y. Baek, Y.-K. Cho, and Y.-H. Kim, Nonlocal dispersion cancellation using entangled photons, Opt. Express **17**, 19241 (2009).

[20] X.-S. Ma, J. Kofler, A. Qarry, N. Tetik, T. Scheidl, R. Ursin, S. Ramelow, T. Herbst, L. Ratschbacher, A. Fedrizzi, T. Jennewein, and A. Zeilinger, Quantum erasure with causally disconnected choice, PNAS **110**, 1221 (2012).

[21] A. N. Black, E. Giese, B. Braverman, N. Zollo, S. M. Barnett, and R. W. Boyd, Quantum nonlocal aberration cancellation, Phys. Rev. Lett. **123**, 143603 (2019).

[22] S. E. Harris, Nonlocal modulation of entangled photons, Phys. Rev. A **78**, 021807(R) (2008).

[23] S. Sensarn, G. Y. Yin, and S. E. Harris, Observation of nonlocal modulation with entangled photons, Phys. Rev. Lett. **103**, 163601 (2009).

[24] S. L. Braunstein and P. van Loock, Quantum information with continuous variables, Rev. Mod. Phys. **77**, 513 (2005).

[25] R. Filip, Continuous-variable quantum erasing, Phys. Rev. A **67**, 042111 (2003).

[26] U. L. Andersen, S. L. Glöck, G. Leuchs, and R. Filip, Experimental demonstration of continuous variable quantum erasing, Phys. Rev. Lett. **93**, 100403 (2004).

[27] V. Händchen, T. Eberle, S. Steinlechner, A. Samblowski, T. Franz, R. F. Werner, and R. Schnabel, Observation of one-way einstein–podolsky–rosen steering, Nature Photonics **6**, 596 (2012).

[28] V. Boyer, A. M. Marino, R. C. Pooser, and P. D. Lett, Entangled images from four-wave mixing, Science **321**, 544 (2008).

[29] R. Filip, L. Mišta, and P. Marek, Elimination of mode coupling in multimode continuous-variable key distribution, Phys. Rev. A **71**, 012323 (2005).

[30] X. Zhu, C.-H. Chang, C. Gonźález-Arciniegas, A. Pe'er, J. Higgins, and O. Pfister, Hypercubic cluster states in the phase-modulated quantum optical frequency comb, Optica **8**, 281 (2021).

[31] R. W. Boyd, *Nonlinear optics* (Academic Press, San Diego, 2008).

[32] V. Boyer, C. F. McCormick, E. Arimondo, and P. D. Lett, Ultraslow propagation of matched pulses by four-wave mixing in an atomic vapor, Phys. Rev. Lett. **99**, 143601 (2007).

[33] K. McKenzie, E. E. Mikhailov, K. Goda, P. K. Lam, N. Grosse, M. B. Gray, N. Mavalvala, and D. E. Mc-

Clelland, Quantum noise locking, J. Opt. B: Quantum Semiclass. Opt. **7**, S421 (2005).

[34] G. Heinzel, A. Rüdiger, and R. Schilling, Spectrum and spectral density estimation by the discrete fourier transform (dft), including a comprehensive list of window functions and some new flat-top windows., Technical Report: Max-Planck-Institut für Gravitationsphysik (Albert-Einstein-Institut), Teilinstitut Hannover (2002).

[35] Q. Glorieux, J. B. Clark, N. V. Corzo, and P. D. Lett, Generation of pulsed bipartite entanglement using four-wave mixing, New J. Phys. **14**, 123024 (2012).

[36] T. Li, B. E. Anderson, T. Horrom, B. L. Schmittberger, K. M. Jones, and P. D. Lett, Improved measurement of two-mode quantum correlations using a phase-sensitive amplifier, Opt. Express **25**, 21301 (2017).

[37] B. Bernard Yurke, S. L. McCall, and J. R. Klauder, SU(2) and SU(1,1) interferometers, Phys. Rev. A **33**, 4033 (1986).

[38] B. E. Anderson, B. L. Schmittberger, T. Gupta, K. M. Jones, and P. D. Lett, Optimal phase measurements with bright- and vacuum-seeded SU(1,1) interferometers, Phys. Rev. A **95**, 063843 (2017).